Transactions of the Illinois Academy of Science
(1987), Volume 80, 1 and 2, pp. 71-82

RESERVOIR CONTROLS IN CARBONATE OFFSHORE BARS, SALEM LIMESTONE (MIDDLE MISSISSIPPIAN), SOUTHEASTERN ILLINOIS

Albert V. Carozzi and Jan L. Reichelderfer
Department of Geology
University of Illinois at Urbana-Champaign
Urbana, Illinois 61801

ABSTRACT

Petrographic and petrophysical studies indicate that the oil- and gas-producing microfacies of the bioclastic and oolitic offshore bars of the Salem Limestone of southeastern Illinois owe their economic properties (porosity reaching 13%) to a complex depositional-diagenetic evolution. The result of this evolution is an association of residual primary submarine porosity and of secondary undersaturated freshwater phreatic porosity which escaped various subsequent cementation processes in the saturated freshwater phreatic and deep burial environments.

No effects of secondary burial dissolution were observed except for very minor fracture and stylolitic porosities.

INTRODUCTION

The Salem Limestone is part of the Middle Mississippian Valmeyeran Series of the Illinois Basin. Its typical bioclastic and oolitic calcarenites in southeastern Illinois belong to shallowing-upward sequences which represent hydrodynamic bars prograding across a gently sloping carbonate ramp. These bars are easily recognizable on geophysical logs, and their origin is attributed to interferences between changes of sea level and regional subsidence (Cluff and Lineback, 1981; Cluff, 1984). Shallowing-upward sequences consist of porous calcarenites underlain and overlain by impermeable calcarenites and calcisiltites which act as reservoir seals. The types of porosity range from primary and primary reduced by pressure solution and cementation to biomoldic and vuggy.

This study attempts to outline how diagenesis generated such a variety of porosity types within typical prograding bioclastic and oolitic bars.

MATERIALS AND METHODS

Sequences representing oil- and gas-producing oolitic and bioclastic bars were investigated in five cores from southeastern Illinois. The cores are listed below by well, location and cored interval.

Core	Well	County	Location	Cored Interval Feet
1	Farrar 5, Roy Reed	Wayne	27-1S-5E	3600-3624
2	Farrar 5, Roy Reed	Wayne	27-1S-5E	3625-3656
3	Farrar 4, Roy Reed	Wayne	27-1S-5E	3593-3643
4	Texaco B-1, Francis Wente	Cumberland	21-9N-7E	2839-2869
5	MEPCO 8, Gray Est	White	30-3S-8E	3805-3828

350 samples were taken at an average vertical interval of 4.5 inches, heated in toluene to eliminate residual hydrocarbons, and impregnated with blue low viscosity epoxy to reveal porosity. Thin sections made from each sample were investigated petrographically and classified into microfacies on the basis of frequencies and types of biogenic and lithic components, proportions and types of matrix and cement, sorting and grain size. Percentages of components, matrix, cement, and porosity were estimated visually using standard charts. Porosity and permeability were measured with Ruska equipment on plugs drilled as close as possible to each thin section location. Porosity terminology is after Choquette and Pray (1970).

Detailed descriptions of the investigated cores and all porosity and permeability measurements are found in Reichelderfer (1985).

RESULTS

The petrographic and petrophysical investigation revealed the existence of nine distinct microfacies which are described in a general and composite shallowing-upward order. However, in reality, two sequences exist with common end-members: an oolitic reservoir bar, and a bioclastic reservoir bar which are lateral hydrodynamic equivalents (See Fig. 3). Possibly these two types of reservoirs may grade laterally into each other within large complex bars, but available control points do not allow demonstration of such a situation.

Graphic representation of the petrographic data (See Fig. 4) corresponds to percentage visual estimation of components (biogenic and lithic), matrix and porosity to which are juxtaposed measured values of porosity in percent using mercury injection method, of permeability in md using nitrogen gas, and an expression of the variations of the relative energy of the environment of deposition.

Microfacies A (slope)

Dolomitized, fine-grained crinoid-*Endothyra* biocalcarenite with bioclastic matrix (Fig. 1A). Large solitary corals and syringoporid corals also occur.

Measured porosity averages 8%, and ranges from 4 to 12%. Primary porosity predominates as unfilled chambers in foraminiferal tests, interseptal spaces in corals, and zooecia of bryozoans. Secondary porosity combines biomolds of unstable constituents (pelecypods and gastropods) held by micrite envelopes, and fractures with intercrystalline porosity in dolomitized matrix. Because of the small size and poorly connected nature of pore spaces, permeability of this microfacies is 0 md. For all practical purposes this microfacies acts as a seal.

Microfacies B (foraminiferal fore bar)

Pressure-welded, *Endothyra*-crinoid biocalcarenite with common syntaxial overgrowths and interparticle sparite cement (Fig. 1B).

Measured porosity averages 9%, and ranges from 2 to 18%. Permeability averages 31 md, and ranges from 0 to 142 md. Primary porosity consists of intraparticle unfilled *Endothyra* chambers, and interparticle reduced by sparite cement and syntaxial overgrowths on crinoid fragments. Abundant overgrowths create a framework that enables pore spaces left by incomplete cementation to remain open. Secondary porosity consists of biomolds of unstable constituents (mollusks) held by micrite envelopes, and fractures. Advanced stages of pressure solution tend to destroy both types of porosity in association with saddle dolomite and anhydrite cements.

Microfacies C (oolitic bar)

Well-sorted compacted oolitic-crinoidal biocalcarenite with isopachous rim cement and interparticle sparite (Fig. 1C). This microfacies is frequently cross-bedded, and locally bioturbated.

Measured porosity averages 13%, and ranges from 3 to 23%. Primary porosity is important as interparticle reduced by isopachous rim and sparite cements, and unfilled chambers of foraminifers. However, in numerous samples porosity is enhanced by secondary types such as biomolds of mollusks, and occasional dissolved ooid concentric laminae (Fig. 2B,C). In samples with maximum porosity of 23%, open vugs of an unusual type due to the dissolution of pelletoidal burrow fillings with microsparite cement (Fig. 2D,E,F) are responsible for most of the porosity because interparticle spaces are highly reduced by calcite cementation. Permeability is often minor (average 22 md, range 0 to 80 md) even when porosity is high because vugs are poorly interconnected. Occlusion of the secondary vug porosity is by sparite, anhydrite, and saddle dolomite (Fig 2G).

Microfacies D (bioclastic bar)

Pressure-welded, crinoidal-algal clast-*Endothyra* biocalcarenite with syntaxial overgrowth cement (Fig. 1D).

Measured porosity averages 10%, and ranges from 1 to 15%. Permeability averages 29 md, and ranges from 0 to 142 md. Primary porosity is important as interparticle reduced either by cementation or pressure solution, and as intraparticle in tests of various organisms. Samples with maximum porosity display a combination of large interparticle unfilled pore spaces, and secondary porosity represented by abundant biomolds of mollusks and oversized pores where several fragments of unstable consti-

tuents were adjacent to each other and dissolved. In some instances, stylolitic and fracture porosities (Fig. 2H) added a small amount of secondary pore space. Advanced stages of pressure solution together with calcite cementation tend to destroy both types of porosity.

Microfacies E (oolitic back bar)

Grain-supported to mud-supported oolitic-algal clast-crinoid-*Endothyra* biocalcarenite with sparite cement, pelletoidal geopetal internal sediment and massive matrix (Fig. 1E). Matrix is locally bioturbated and isopachous rim cement is also present.

Measured porosity averages 8%, and ranges from 3 to 11%. Permeability averages 14 md, and ranges from 0 to 51 md. Primary porosity generally predominates as reduced type by incomplete calcite cementation. Secondary porosity is again responsible for the highest value of 11% as the unusual type of open vugs due to the dissolution of pelletoidal burrow fillings (as in microfacies C) together with biomolds of mollusks, dissolved concentric layers of ooids, and stylolitic porosity. Samples with lesser porosity are either pressure welded, or finer grained, and contain abundant crinoids with syntaxial overgrowths.

Microfacies F (bioclastic back bar)

Fine-grained crinoid-*Endothyra* biocalcarenite with pelletoidal matrix and interparticle sparite cement (Fig. 1F). Matrix is frequently geopetal.

Measured porosity is 3% and entirely primary reduced by incomplete interparticle cementation. Permeability is 0 md.

Microfacies G (reworked algal flat)

Grain-supported algal-(*Stachyodes*, *Girvanella* and *Orthonella*) crinoidal biocalcarenite with isopachous rim cement and interparticle sparite (Fig. 1G).

Measured porosity averages 7%, and ranges from 1 to 12%. Permeability averages 13 md, and ranges from 0 to 53 md. Primary porosity predominates generally as reduced type by a combination of submarine dissolution of isopachous rim cement, and incomplete interparticle sparite cementation. Samples with lesser porosity display fibrous rim cement which occluded most of the primary porosity. Minor secondary porosity consists of pelecypod biomolds. Destruction of porosity results from a sparite mosaic cement, sometimes associated with saddle dolomite filling any remaining pore space except for an occasional incompletely cemented pelecypod biomold.

Microfacies H (algal flat)

Algal-constructed to grain-supported algal clast-oolitic-crinoidal biocalcarenite with isopachous rim cement, geopetal pelletoidal internal sediment, and sparite cement (Fig. 1H).

In situ algal growths of *Girvanella*, *Orthonella*, and *Stachyodes* characterize this microfacies, together with large algal-coated intraclasts. Geopetal internal sediment rests on isopachous rim cement showing partial submarine dissolution, and on a variety of components.

Measured porosity averages 8%, and ranges from 2 to 12%. Permeability is negligible (average 0 md, range 0 to 2 md). Primary porosity predominates as reduced type by isopachous rim and sparite cement. Secondary porosity consists of partially

dissolved normal ooids, and large vugs due to the dissolution of pelletoidal matrix filling of burrows. Samples with lesser porosity result from a combination of abundant pelletoidal matrix, thick isopachous rim cement, and well-developed sparite cement. The latter together with saddle dolomite fill interparticle voids and dissolution vugs.

Microfacies I (lagoon)

Bioturbated, fine-grained, mud-supported crinoid-ostracod-calcisphere-small benthic foraminifer biocalcarenite with argillaceous calcisiltite and bioclastic matrix (Fig. 2A). Bioturbation and pyrite streaks are common.

Measured porosity is 1%, but no porosity is visible in thin section. Permeability is 0 md, and for all practical purposes this microfacies acts as a seal. Primary porosity represented by minute interparticle pore spaces, and intraparticle spaces in tests as well as secondary porosity corresponding to biomolds have been occluded by microsparite cement.

Ideal Depositional Models

In both bioclastic and oolitic bars, microfacies A representing the slope is dolomitized. This dolomitization took place probably soon after deposition by a dorag process resulting from freshwater and marine water mixing. However, no evidence of the exposure necessary to provide freshwater for dolomitization has been encountered in the investigated sections. It is known that minor subaerial exposure of carbonate bodies could provide temporary and localized conditions of mixing (Kaldi and Gidman, 1982). Therefore, the assumption is made that some of the bars could have been exposed occasionally.

In the ideal bioclastic bar model (Fig. 3A), the amount of matrix varies in clear opposition to porosity and permeability. Both well-sorted calcarenite microfacies B and D with peaks of porosity and permeability display predominantly interparticle reduced primary porosity. Where matrix is present, as in the slope (A), bioclastic back bar (F), and lagoon (I) microfacies, porosity and permeability are reduced.

The relationship between porosity, permeability, and microfacies is more complex in the ideal oolitic bar model (Fig. 3B). The oolitic bar (microfacies C), which shows the greatest porosity, contains numerous oolitically coated crinoids. This texture makes syntaxial overgrowths on crinoids rare. Although they reduce primary porosity when present, these overgrowths formed a stable framework that kept residual pore space open during pressure solution. Vugs also add to the porosity in this microfacies. The peak in permeability, however, is in the foraminiferal fore bar (microfacies B) because the chambers in the *Endothyra* provide numerous interconnected pore spaces.

Although matrix certainly influences the reduction of porosity and permeability in the slope (A) and lagoonal (I) microfacies, other matrix-rich microfacies, such as the oolitic back bar (E), still display high porosity. This porosity is related to the formation of vugs by burrow dissolution. Although algal flat microfacies (H) displays matrix, it also contains interstitial calcarenite where most of the porosity is located. Unfilled vugs add to the porosity in this microfacies, but because they are poorly interconnected, they often do not affect permeability.

In summary, both types of bars contain good reservoir microfacies represented by the uncompacted, well-sorted, coarse-grained oolitic calcarenites (porosity 13%),

bioclastic calcarenites (porosity 10%), and foraminiferal calcarenites (porosity 9%). Lower energy microfacies which underlie and overlie the reservoirs represent environments in front and in the back of the hydrodynamic bars which are matrix-rich, finer grained, and act as seals.

A typical example of shallowing-upward bioclastic bar sequence is the core from the well Texaco B-1, Francis Wente (Fig. 4) in which porosity is confined to the coarse-grained foraminiferal and bioclastic bars (microfacies B,D). In the coarse-grained samples from 2856 to 2848 feet, porosity can be related to moderate pressure solution, especially where overgrowths on crinoid fragments show partially infilled pore space and created a stable framework that did not allow primary pore space to collapse during pressure solution.

The largest values of porosity and permeability occur when unfilled foraminiferal tests are abundant and provide additional pore space. In samples with abundant overgrowths, components are more often sutured and no pore space is left. In the finer grained samples, overgrowths tend to occlude all primary porosity.

DISCUSSION AND CONCLUSION

A generalized diagenetic sequence can be prepared encompassing all the investigated cores (Fig. 5), and explaining the origin of the porosity of the oil- and gas-producing microfacies of the bioclastic and oolitic bars.

The petrographic description of microfacies shows that the main type of porosity is primary interparticle and intraparticle in part immediately reduced by isopachous rim cementation which takes place in the active marine phreatic environment. Further porosity of secondary type is generated by total or partial dissolution of unstable aragonitic or high-magnesium constituents such as tests of pelecypods and gastropods surrounded by micrite envelopes, pelletoidal filling of burrows with submarine microsparite cement, and concentric rings of ooids. This process occurred in the undersaturated freshwater phreatic environment. A small amount of intercrystalline secondary porosity developed through a dorag process of dolomitization in the slope microfacies, and was accompanied by secondary quartz generation.

Early compaction caused minor fracturing, and these early fractures are difficult to distinguish from those of late burial origin. Petrographically, the cements filling the fractures do not appear different, nor could cathode luminescence distinguish between them. The fracture morphology (an even, straight fracture formed during early compaction and a fibrous, branching fracture formed during the more ductile burial stage) usually allows them to be differentiated. The relationship of stylolites to fractures also contributes to the distinction: early compaction fractures are sometimes cut by stylolites, whereas late fractures seem to be associated with the process of stylolitization.

Further subsidence of the microfacies into the saturated freshwater phreatic environment led to widespread cementation of all previous types of porosity by interparticle sparite mosaic and syntaxial overgrowths (sparite cementation I).

In the burial environment cementation continued through the action of formation brines as silicification, anhydritization, and precipitation of saddle dolomite as well as some late sparite in fractures (sparite cementation II). The timing of these processes of cementation varies, but silicification seems to precede anhydritization as shown by silicified crinoid fragments replaced by anhydrite. At least two phases

of anhydritization are evident: pore filling and replacive. The second phase replaces saddle dolomite, but in another sample, a rhomb of saddle dolomite replaces massive anhydrite. Both saddle dolomite and anhydrite can replace components, matrix, and cement pervasively or act as a pore-filling cement. The reducing conditions in the burial environment probably also account for the reduction of the residual organic matter in *Endothyra* and other bioclasts to form pyrite. During burial which reached 6000 feet or more during Late Pennsylvanian or Permian (Damberger, 1971), and is now approximately 2000 to 4000 feet, no important dissolution processes took place with the exception of very minor generation of fracture and stylolitic secondary porosities. Present-day porosity of economic interest in the Salem Limestone consists of pores which have survived the complex diagenetic evolution described above.

ACKNOWLEDGEMENTS

The authors are grateful to Chevron Oil Company, Texaco U.S.A., and Sigma Xi, the Scientific Research Society for financial support of this investigation. Thanks are due to Dr. Daniel B. Blake for critical reading and constructive discussions. Samples were generously provided by the Illinois State Geological Survey.

LITERATURE CITED

Choquette, P.W. and L.C. Pray, 1970. Geologic nomenclature and classification of porosity in sedimentary carbonates. Bull. Am. Assoc. Petrol. Geologists. 54(2):207-250.

Cluff, R.M., 1984. Carbonate sand shoals in the Middle Mississippian (Valmeyeran) Salem — St. Louis — Ste. Genevieve Limestones, Illinois Basin. *In* Carbonate sands — a core workshop (P.M. Harris, ed.). Soc. Econ. Paleontologists and Mineralogists, core workshop No. 5. 94-135.

Cluff, R.M. and J.A. Lineback, 1981. Middle Mississippian carbonates of the Illinois Basin: a seminar and core workshop. Illinois Geological Society, 88 pp.

Damberger, H., 1971. Coalification pattern of the Illinois Basin. Econ. Geology. 66(3):488-494.

Kaldi, J. and J. Gidman, 1982. Early diagenetic dolomite cements: examples from the Permian Lower Magnesian Limestone of England and the Pleistocene carbonates of the Bahamas. Jour. Sed. Petrology. 52(4):1073-1085.

Reichelderfer, Jan. L., 1985. Microfacies, diagenesis, and porosity development in the Salem Limestone (Middle Mississippian), southern Illinois, U.S.A. Unpublished M.S. Thesis, University of Illinois, Urbana-Champaign, 95 pp.

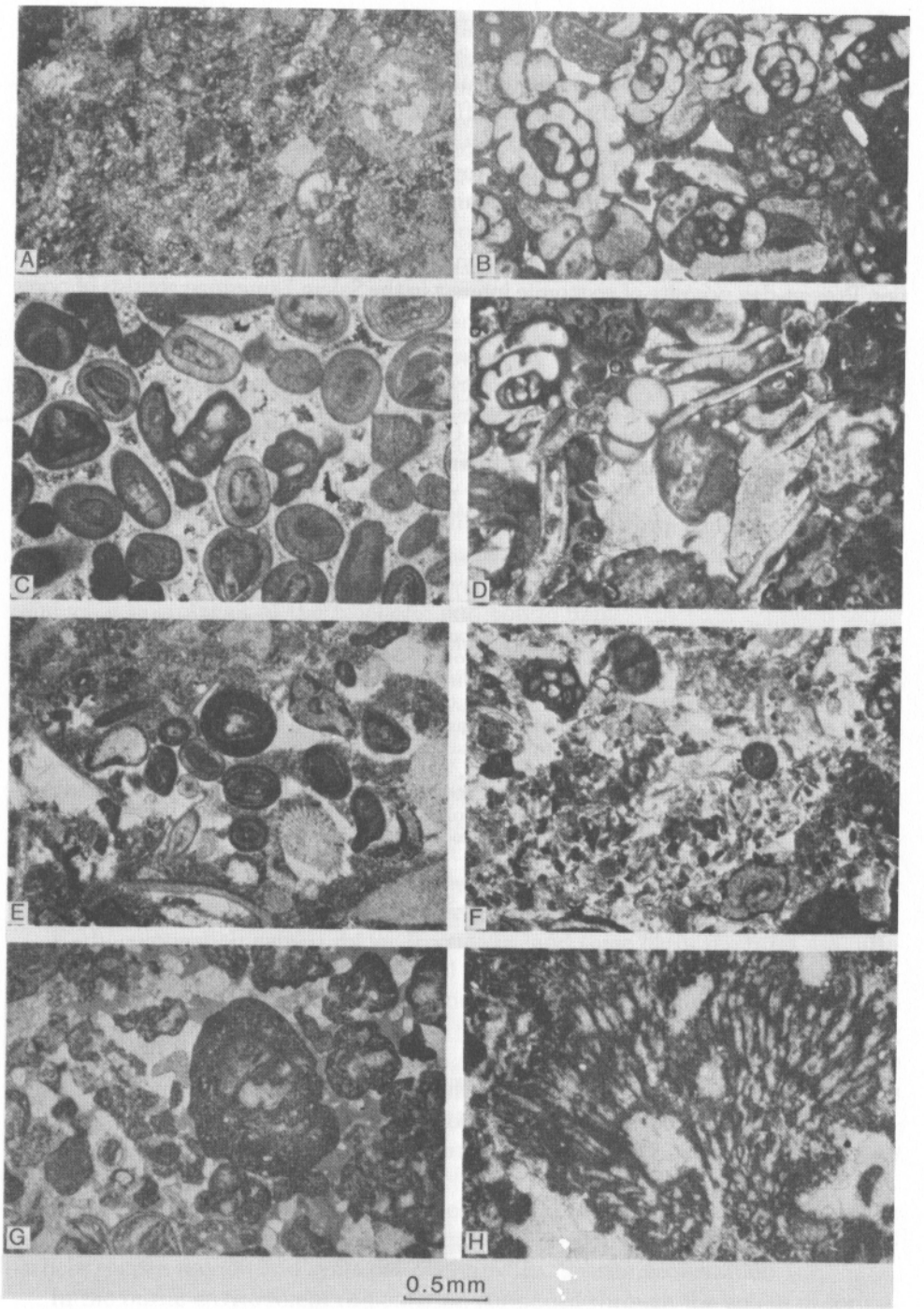

Fig. 1. Typical microfacies. A. Microfacies A. B. Microfacies B. C. Microfacies C. D. Microfacies D. E. Microfacies E. F. Microfacies F. G. Microfacies G. H. Microfacies H. All photomicrographs: plane polarized light, except C, crossed nicols.

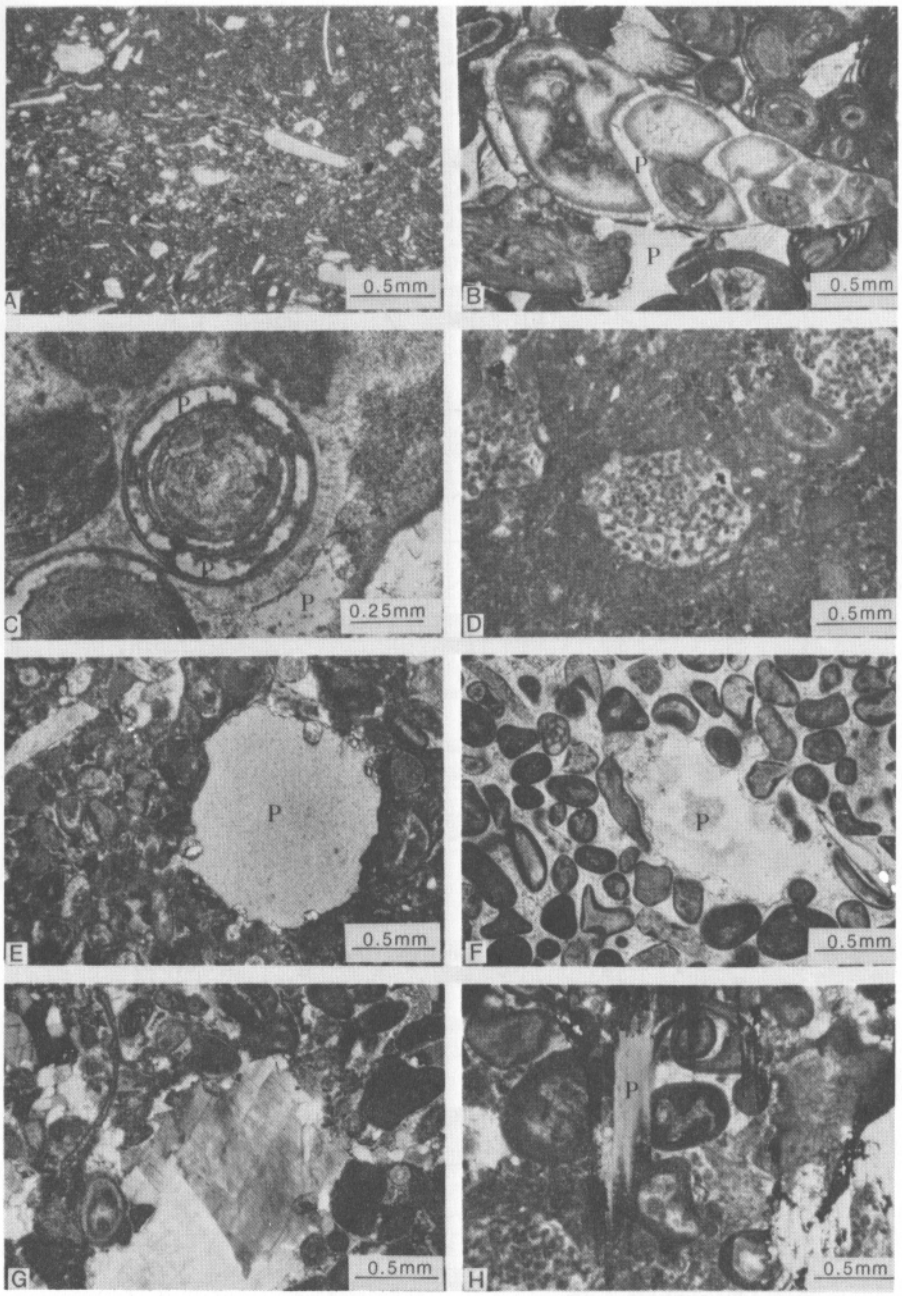

Fig. 2. Typical microfacies (continued) and porosity types (designated by letter P). A. Microfacies I. B. Partially filled gastropod biomoldic porosity and reduced interparticle porosity. C. Selective cortical dissolution in ooid, with compacted submarine fibrous rim cement. D. Burrows filled with pellets and submarine microsparite cement. Vugs illustrated in E, F, and G similarly are inferred to have been filled before dissolution. E. Unfilled vug, with lack of interstitial porosity in biocalcarenite. F. Unfilled vug, with well-preserved rim cement surrounding ooids and bioclasts near vug and dissolution of mollusk fragment to right of vug. G. Vug filled with saddle dolomite and minor sparite. H. Stylolitic porosity. All photomicrographs: plane polarized light, except G, crossed nicols.

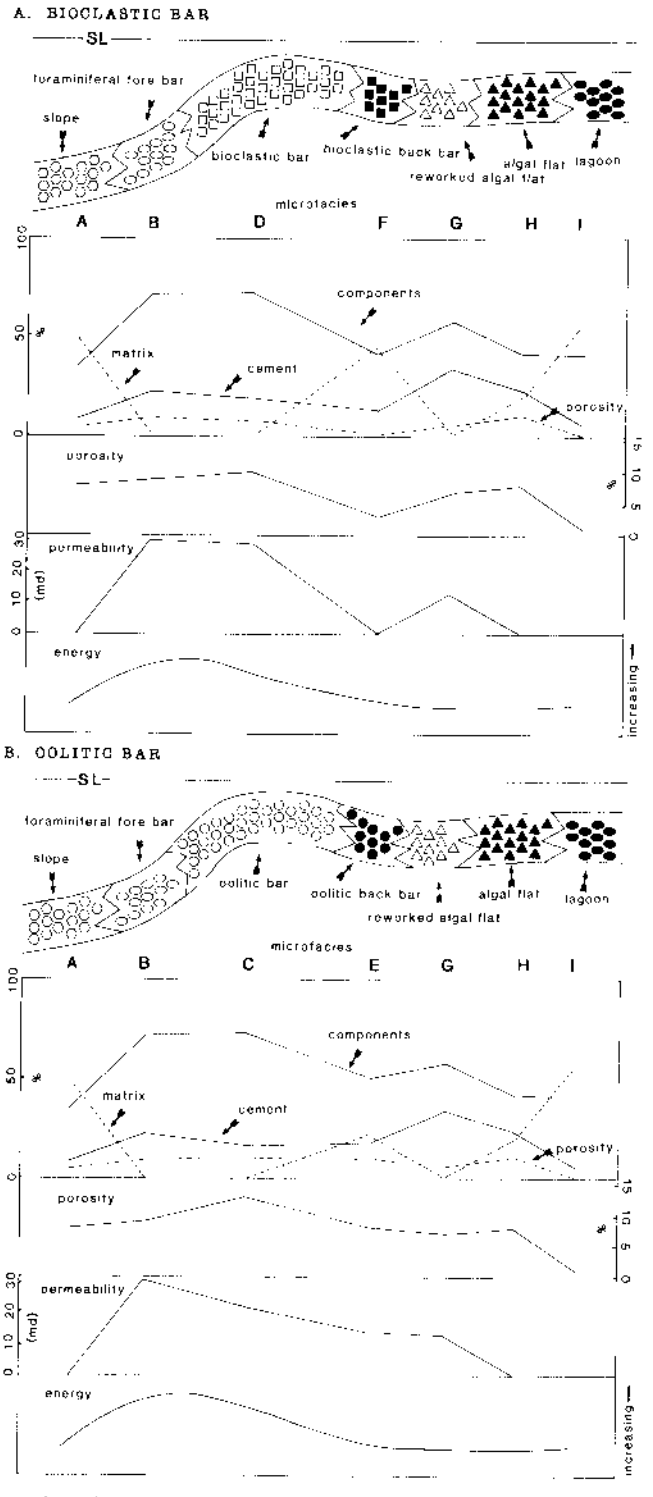

Fig. 3. Ideal depositional models.

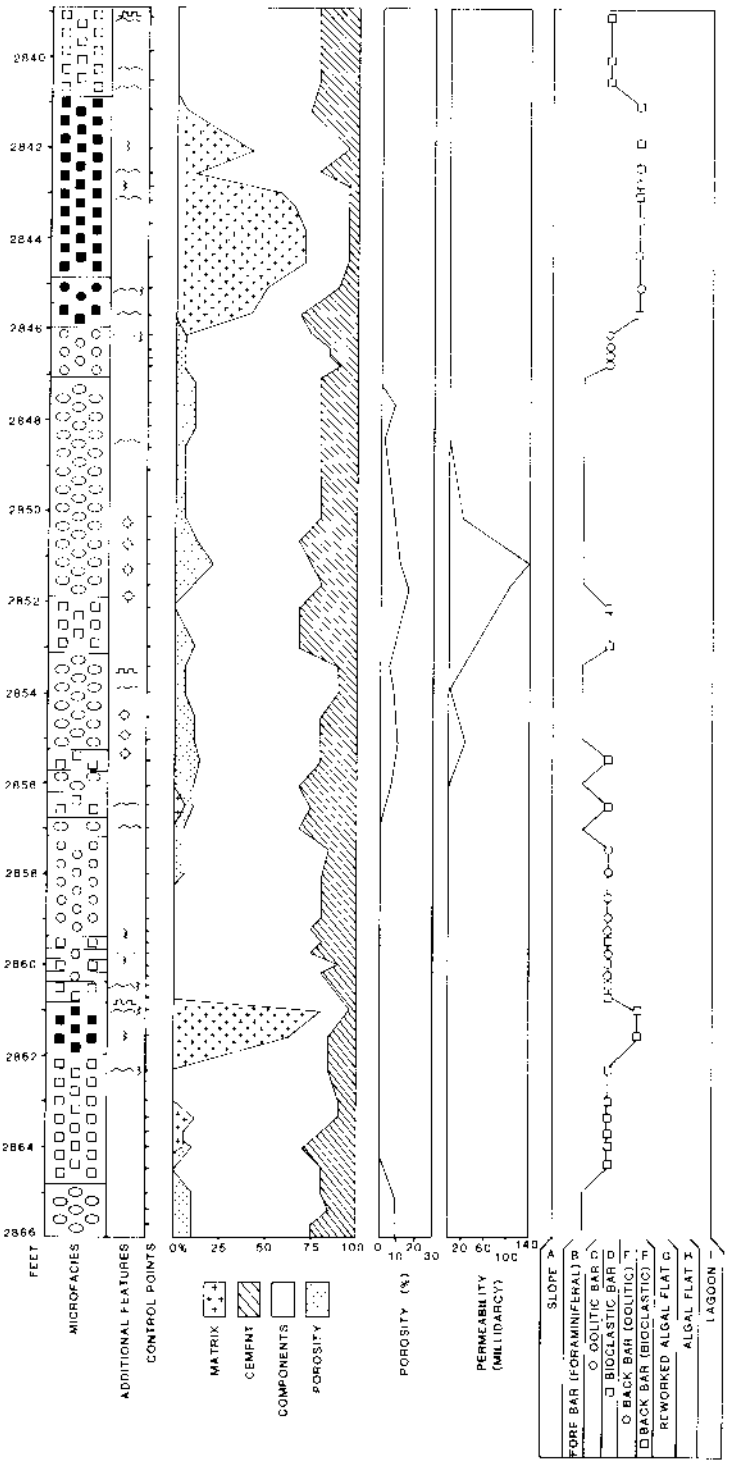

Fig. 4. Typical vertical variation of microscopic parameters during shallowing-upward sequence, well Texaco B-1, Francis Wente.

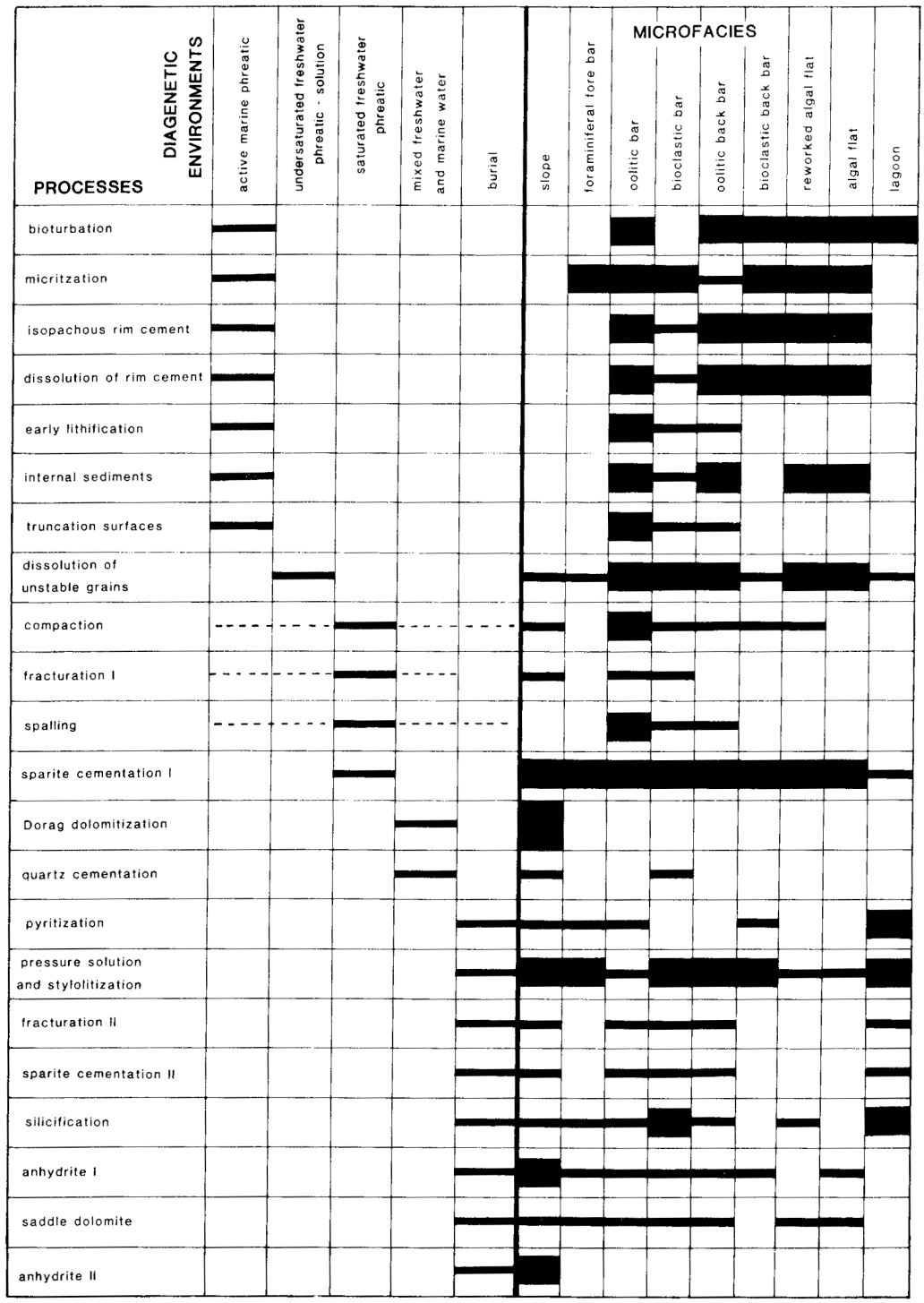

Fig. 5. Summary of diagenetic processes and environments. Thickness of line denotes comparative abundance of process in microfacies.